ISSN NO : 2230-7850 IMPACT FACTOR : 5.1651 (UIF) VOLUME :8, ISSUE : 9, OCTOBER - 2018

INDIAN STREMS RESEARCH JOURNAL

Robust PI-PD Controller Design: Industrial Simulation CaseStudies and a Real-Time Application

Dr. Rekha

Assistant professor in Electronics Government college (Autonomous)

Kalaburagi.

Abstract: *When it comes to regulating and integrating industrial processes with temporal delays, PI-PD controllers outperform typical PID controllers. It is not simple to calculate the four tuning parameters for this kind of controller, though. Determining the tuning criteria for PI-PD controllers that make use of the stability zone has garnered a lot of attention lately. The majority of PI-PD controller tuning rules are now displayed graphically, which can be time-consuming and hinder their industrial application. To overcome this deficiency, there aren't enough analytical tuning suggestions in the literature. However, a rigorous design approach is not taken into account by the current analytical tuning standards. New robust analytical tuning criteria based on preset gain and phase margin limitations are proposed in this work.*

Keywords: PI-PD controller; stability region; robust control; centroid point; DC–DC buck converter; DC motor; heat exchanger; twin rotor multi-input multi-output system

1. Introduction

The literature makes considerable use of the second order plus time delay (SOPTD) system model because it faithfully captures the dynamics of many real-world industrial applications, including DC motors and temperature controllers. Long delays, however, exacerbate the control issues with these systems since they lead to ambiguity and delayed reactions with greater overshoots. The control design challenge is further complicated by the existence of poles at the origin of the s-plane or on the right side. Thus, to regulate such systems, a strong control strategy is needed [1].

Compared to PID controllers, PI-PD controllers are better options for resolving the control issues highlighted above [2]. They change a process's poles to a more neutral state by using the PD portion of an inner feedback loop. Those four parameters [6]. In addition, compared to PID controllers, this controller's design has received comparatively less study attention [7]. Therefore, more research on this type of controller is still necessary.

Utilizing the stability region approach to calculate all stabilizing controller gains is a widely researched topic (see [8–11] for examples). Since it provides straightforward and useful tuning guidelines and gets around the challenge of tuning the PI-PD controller, many researchers have recently explored using the centroid point of the stability region, which can be calculated by using the centroid of convex stability region (CCSR) [12] or the weighted geometrical center (WGC) approaches [13,14], to adjust the parameters of PI-PD controllers. Additionally, it has been suggested that the controller evaluated using the centroid point may produce robustness against parameter fluctuations, faster perturbation rejection, and improved set-point tracking [15,16]. WGC and CCSR have just lately been used to graphically adjust the PID controller's gains, which are intended to control systems with non-integer order delay [17]. Additionally, a comparison study of the PI-PD controller tuning techniques employing CCSR and WGC has recently been conducted [14]. Because CCSR and WGC approaches have only been applied to specified transfer functions in the above-mentioned literature, they share the common drawback of requiring the design pro- cess to be repeated whenever the transfer function changes. This might be time-consuming for controller engineers and might require mathematical knowledge. The user-selected step size to be employed in the design phase causes a computational load, which is a unique drawback of the WGC approach [12]. Additionally, if the time lag is particularly significant, the WGC approach may yield an incorrect centroid location because of its sensitivity to the chosen step size [18]. The graphical way of determining the centroid location is a drawback unique to the CCSR approach [4]. Additionally, novel methods for determining a fractional order controller's stability region's centroid point have recently been introduced [19,20]. In addition, the centroid point has recently been used in the controller parameter design for DC–DC boost converters [21]. Nevertheless, the centroid point is still obtained graphically in all of the aforementioned stated approaches, which is laborious.

To remove the above-mentioned disadvantages of centroid point approaches, analyti- cal tuning rules have been recently suggested [3,4,16,18,22]. However, these approaches have not considered incorporating a centroid point based on a robust design method. In fact, since the original work that formulated the stability region's formulas for time delay systems and PI-PD controllers, as documented in Ref. [23], the majority of researchers have tuned these controllers using graphical approaches without taking analytical ones into account. Furthermore, robust design techniques as previously discussed have not taken into account analytical methodologies. Therefore, the main goal of this paper is to design a robust tuning rule based on the centroid point, which can specifically withstand the system parameter uncertainties and provide acceptable settling times and overshoots. The primary contributions made by this work are:

1. Relative to the centroid point approaches reported in Refs. [3,4,16,18,22], the proposed method incorporates a robust design approach based on predefined gain and phase margin boundaries, which gives the designer more flexibility to obtain the desired control performances.
2. Relative to the centroid point approaches reported in Refs. [12,14,19,20], the proposed methods are analytical and not graphical, which saves time and is easy to implement on the industrial level.
3. Compared to the centroid point derived based on a robust design technique for DC–DC converter control published in Ref. [24], the suggested approach is analytical and does not call for any graphical adjustments. Furthermore, any system that can be represented as a stable SOPTD can use the suggested approach.

To conclude, proposing an analytical robust design method for designing the gains of the PI-PD controller is the main contribution of this paper. This is the layout for the rest of the paper. The next part explains the PI-PD controller structure. The suggested methodology is expounded upon in Section 3. Section 4 describes the simulation and thereal-time results. The last section deals with conclusions.

2. PI-PD Controller Structure

Every action taken by the PID regulator in a traditional closed-loop system occurs via the forward path. This can cause an unwanted occurrence known as a derivative kick. To solve this issue, the PD part of PI-PD regulators is moved to an internal feedback loop, which moves the poles of the plant transfer function to a more favorable location where the PI component operating in the onward path might more adequately control it [4,18]. The PI-PD regulator's architecture is shown in Figure 1. The inner loop is composed of the transfer functions of the plant, $G(s)$, and the PD controller, $C_{PD}(s)$, whereas the external loop is composed of the transfer functions of the inner loop and the PI regulator, $C_{PI}(s)$. The transfer functions $C_{PD}(s)$ and $C_{PI}(s)$ of the PI-PD regulator are written as follows:

$$C_{PD}(s) = k_f + k_d s \tag{1}$$

$$C_{PI}(s) = k_p + \frac{k_i}{s} \tag{2}$$

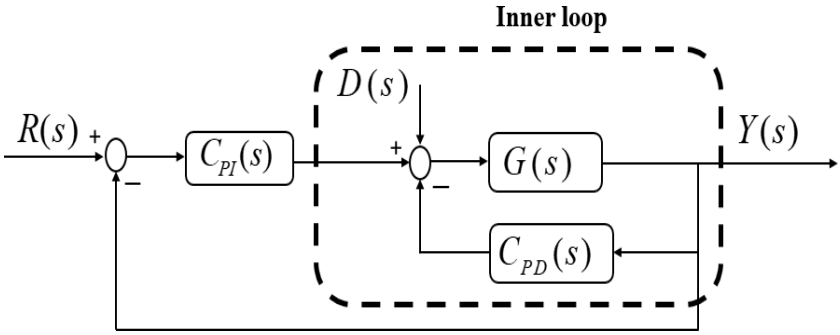

Figure 1. PI-PD controller.

The behavior of many industrial plants can be described as a second-order transfer function with time delays as follows:

$$G(s) = \frac{Ke^{-\tau s}}{as^2 + bs + c} \tag{3}$$

In the above equation, the time delay, the process gain, and the coefficients of the transfer function are τ, K, a, b, and c, respectively.

3. Proposed Approach

The gain-phase margin tester, $T(s) = Ae^{-\phi s}$, is added to the forward path to find boundaries in the general stability boundary corresponding to the predetermined gain and phase margins. Figure 2 shows the structure of the PI-PD controller after adding the tester [23].

The following closed-loop characteristic equation can be used to characterize the inner feedback loop shown in Figure 2, which is made up of the PD controller transfer function, $C_{PD}(s)$, and the process transfer functions, $G(s)$:

$$\Delta(s) = 1 + C_{PD}(s)G(s) \Rightarrow \Delta(s) = k_f Ke^{-\tau s} + k_d Kse^{-\tau s} + as^2 + bs + c \tag{4}$$

In the parameter space methodology, the root of a stable polynomial has three ways of crossing over the imaginary axis and becoming unstable. The real root boundary, the infinite root boundary, and the complex root boundary are the three boundaries that these ways define [4]. To find the real root boundary, we solve Equation (4) with $s = 0$ and $\Delta(s) = 0$. Therefore, $k_f = -c/K$ defines the boundary. Since the controller parameters are absent from the coefficient of s^2, the infinite root boundary cannot be part of the stability region. To find the complex root boundary, we enter $s = j\omega$, $e^{-j\tau\omega} = \cos(\tau\omega) - j\sin(\tau\omega)$, and $j = \sqrt{-1}$ into Equation (4) as given below:

$$\Delta(s) = -a\omega^2 + jb\omega + c + k_f K\cos(\tau\omega) - jk_f K\sin(\tau\omega) + jk_d K\omega\cos(\tau\omega) + k_d K\omega\sin(\tau\omega) = 0 \tag{5}$$

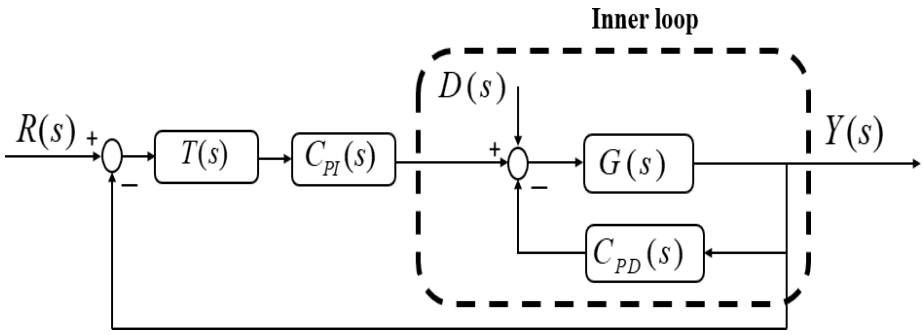

Figure 2. PI-PD controller plus gain-phase margin tester.

The imaginary and real components in Equation (5) are then split and equaled to zero.

Consequently, the following equations can be obtained:

$$k_d(\omega\cos(\tau\omega)) - k_f(\sin(\tau\omega)) = -\frac{b}{K}\omega \tag{6}$$

$$k_d(\omega\sin(\tau\omega)) + k_f(\cos(\tau\omega)) = \frac{a\omega^2 - c}{K} \tag{7}$$

The expressions that follow can be obtained by solving Equations (6) and (7) for k_d and k_f:

$$k_d = \frac{1}{K}\left(-b\cos(\tau\omega) + \left(a\omega - \frac{c}{\omega}\right)\sin(\tau\omega)\right) \tag{8}$$

$$k_f = \frac{1}{K}\left(a\omega^2 - c\right)\cos(\tau\omega) + b\omega\sin(\tau\omega) \tag{9}$$

The inner feedback loop's stability region is defined by Equations (8) and (9) and the line $k_f = c/K$. By varying ω throughout the range of ε ω_{PD}, Equations (8) and (9) are utilized to construct the stability region. ε is a small number that is used to avoid dividing by zero in Equation (8), while ω_{PD} is found by taking the first root of the equation: $(a\omega^2 - c)\cos(\tau\omega) + b\omega\sin(\tau\omega) = -c$. The adjusting point of the PD controller can be found using the mathematical relations in the range of e f [18]:

$$\bar{x} = \frac{1}{f-e}\int_e^f z(x)dx \tag{10}$$

$$\bar{y} = \frac{1}{2(f-e)}\int_e^f g(x)dx \tag{11}$$

The integrations provided in Equations (10) and (11) should be used to analytically calculate the settings of the PD controller. Also, the same mathematical relations will be used later for finding the settings of the PI controller. Considering $f = \omega_{PD}$, $e = 0$, and $z(x) = k_d$ which is given in Equation (8), and $g(x) = k_f$ which is given in Equation (9), the gains of the PD controller are analytically computed using Equations (10) and (11). Thus, the following expressions are obtained and used to find the setting of this controller:

$$k^* = \frac{1}{K\omega_{PD}}\left[\frac{a(\sin(\tau\omega_{PD}) - \tau\omega_{PD}\cos(\tau\omega_{PD}))}{\tau^2} - \frac{b\sin(\tau\omega_{PD})}{\tau} - c\left(\frac{\tau^6\omega_{PD}^5}{600} - \frac{\tau^4\omega_{PD}^3}{18} + \tau^2\omega_{PD}\right)\right] \tag{12}$$

$$k_f^* = \frac{1}{2K\omega_{PD}} \frac{b(\sin(\tau\omega_{PD}) - \tau\omega_{PD}\cos(\tau\omega_{PD}))}{\tau^2} + \frac{(\tau^3(a\omega_{PD}^2 - c) - 2a)\sin(\tau\omega_{PD}) + 2a\tau\omega_{PD}\cos(\tau\omega_{PD})}{\tau} \quad (13)$$

Here, it is important to illustrate that the first three terms of the Taylor series are used for approximation $\frac{\tau\sin(\tau\omega)}{\tau\omega}$ and consequently achieving the integration action in Equation (13). The first three terms of the Taylor series are selected as they can provide good computation accuracy without introducing mathematical complexity. To compute the controller parameters using Equations (12) and (13), one should first identify the parameters of the SOPTD system reported in Equation (3). After that, ω_{PD} should be computed by taking the first root of the equation: $(a\omega^2 - c)\cos(\tau\omega) + b\omega\sin(\tau\omega) = c$. This can be achieved by using a scientific package such as MATLAB.

To find the PI controller parameters k_i^* and k_p^*, the outer loop's characteristic equation is given below:

$$\Delta(s) = 1 + G_{PD}(s)G(s) + Ae^{-j\phi}G_{PI}(s)G(s) = as^3 + bs^2 + cs + AKk_p^* se^{-j(\tau\omega+\phi)} + AKk_i^* e^{-j(\tau\omega+\phi)} + Kk_f^* se^{-\tau s} + Kk_d^* s^2 e^{-\tau s} \quad (14)$$

Afterward, the real root boundary, the infinite root boundary, and the complex root boundary are determined. For the outer loop, the real root boundary is found by solving Equation (14) for $s = 0$ and $\Delta(s) = 0$. Thus, this boundary is defined by $k_i = 0$. The infinite root boundary cannot be a component of the stability zone since the controller's settings are missing from the coefficient of s^3. The complex root boundary is found by entering $s = j\omega$, $e^{-j\tau\omega} = \cos(\tau\omega) - j\sin(\tau\omega)$, $e^{-j\phi} = \cos(\phi) - j\sin(\phi)$, and $j = \sqrt{-1}$ into Equation (14). After that, imaginary and real components are split to obtain the following equations:

$$k_p(\omega\sin(\tau\omega + \phi)) + k_i(\cos(\tau\omega + \phi)) = \frac{b}{AK}\omega^2 - \frac{k_f^*}{A}\omega\sin(\tau\omega) + \frac{k_d^*}{A}\omega^2\cos(\tau\omega) \quad (15)$$

$$k_p(\omega\cos(\tau\omega + \phi)) - k_i(\sin(\tau\omega + \phi)) = \frac{a}{AK}\omega^3 - \frac{c}{AK}\omega - \frac{k_f^*}{A}\omega\cos(\tau\omega) - \frac{k_d^*}{A}\omega^2\sin(\tau\omega) \quad (16)$$

The complex root boundary's equations are given by solving Equations (15) and (16) for k_p and k_i as follows:

$$k_p = \frac{\frac{b}{AK}\omega^2\cos(\tau\omega + \phi) + \frac{k_f^*}{A}\omega\sin(\tau\omega)\sin(\tau\omega + \phi) - \frac{k_d^*}{A}\omega^2\cos(\tau\omega)\sin(\tau\omega + \phi)}{\frac{b}{AK}\omega^2\sin(\tau\omega + \phi)} \quad (17)$$

$$k_i = \frac{\frac{a}{AK}\omega^3\sin(\tau\omega + \phi) - \frac{c}{AK}\omega\sin(\tau\omega + \phi) + \frac{b}{AK}\omega^2\cos(\tau\omega + \phi) + \frac{k_f^*}{A}\omega\cos(\tau\omega)\sin(\tau\omega + \phi) - \frac{k_d^*}{A}\omega^2\cos(\tau\omega)\cos(\tau\omega + \phi)}{\frac{b}{AK}\omega^2\sin(\tau\omega + \phi)} \quad (18)$$

The line $k_i = 0$ and Equations (17) and (18) are used to determine the stability region of the outer loop. To plot Equations (17) and (18), ω is changed throughout the range of $0 \ \omega_{PI}$, where ω_{PI} is found by equating Equation (18) to zero and taking the first solution. After applying the formulae from Equations (10) and (11) to Equations (17) and (18), correspondingly, the settings of the PI controller are determined as follows:

$$k_p = \frac{1}{\omega_{PI}} \cdot \left(\frac{\left(2a\tau^2\omega_{PI}^2 - 2c\tau^2 + 2b\tau - 4a\right)\sin(\tau\omega_{PI}+\phi) + \left(4a\tau - 2b\tau^2\right)\omega_{PI}\cos(\tau\omega_{PI}+\phi)}{2AK\tau^3} + \frac{Kk_d\tau^3\omega_{PI}^2\sin(\phi) - 2Kk_f\tau^3\omega_{PI}\cos(\phi)}{2AK\tau^3} + \frac{\left(2c\tau^2 - 2b\tau + 4a\right)\sin(\phi)}{2AK\tau^3} \right) \cdot \quad (19)$$

$$k_i = \frac{1}{2\omega_{PI}} \left(\frac{\left((6b\tau^3 - 18a\tau^2)\omega_{PI}^2 + 6c\tau^2 - 12b\tau + 36a\right)\sin(\tau\omega_{PI} + \phi)}{6AK\tau^4} + \frac{\left(6a\tau^3\omega_{PI}^3 + \left(-6c\omega_{PI}\tau^3 + 12b\tau^2 - 36a\tau\right)\omega_{PI}\right)\cos(\tau\omega_{PI} + \phi)}{6AK\tau^4} + \frac{+2Kk_d\tau^4\cos(\phi)\omega_{PI}^3 + 3Kk_f\tau^4\sin(\phi)\omega_{PI}^2 - \left(6c\tau^2 - 12b\tau + 36a\right)\sin(\phi)}{6AK\tau^4} \right) \quad (20)$$

One can find the controller parameters using the flowchart shown in Figure 3. Here, it is important to mention that no approximations have been used to find Equations (19) and (20).

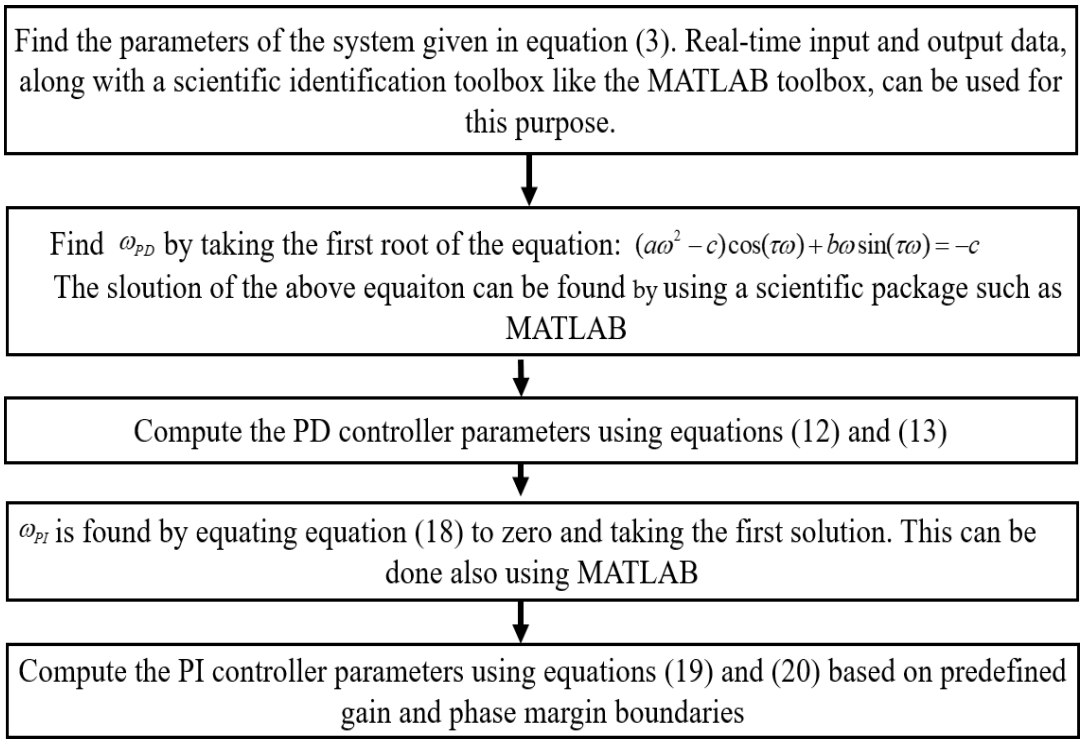

Figure 3. The flowchart for finding the PI-PD parameters using the proposed method.

4. Simulation and Real-Time Case Studies

Three simulation case studies and a real-time application will be shown in this section. The PD controller's derivative component with the form $C_{PD}(s) = k_f + k_d s/(t_f s + 1)$, where $t_f = (k_d)/(10k_f)$, is used for noise rejection and practical application. To ensure a fair comparison with the methods in the literature, the derivative filter will also be introduced to all literature techniques under consideration. The examined approaches are numerically evaluated using the gain margin, the phase margin, the integral of absolute error (IAE), $IAE = \int_0^\infty |e|dt$, and the total variation (TV), $TV = \int_0^\infty (u(t+1) - u(t))dt$.

Case study 1: A DC–DC buck converter, which is shown in Figure 4, is studied here. The identified transfer function of this system is $G(s) = \frac{8.87e^{-2\times10^{-4}s}}{7.0341\times10^{-7}s^2 + 0.0017s + 1}$ [25]. The suggested method for different predefined gain and phase margin boundaries is applied to find out the controller settings using the procedures shown in Figure 3. Table 1 summarizes these settings' values as well as the PID controller's values reported in Reference [25].

Figures 5 and 6 show the stability region with computed centroid points using the proposed method for inner and outer loops, respectively. Figure 6 shows the stability region for three predefined scenarios of the gain and phase margin boundaries, which are $A = 1 \quad \phi = 0°$, $A = 1.5 \quad \phi = 0°$, and $A = 1.6 \quad \phi = \pi/4°$. The scenario corresponding to $A = 1 \quad \phi = 0°$ means that no gain and phase margin boundaries are included in the design of the centroid point. First, the described controllers are assessed using the system parameters' nominal values. Specifically, at t = 0 s, the system is given

a unity step input. Additionally, at t = 0.02 s, a disturbance with an amplitude of 0.3 is introduced into the closed-loop system. Figure 7 illustrates the output voltage responses of the assumed scenarios along with the PID [25] and their control signals. From the figure, all the proposed scenarios give better results in terms of generating small overshoots relative to the PID controller [25], which appears to consume more energy with possible oscillation, as is clear in Figure 7b. In fact, the overshoot and observed oscillations of the PID controller [25] might be a source of instability in practical implementations. On the other hand, the proposed method does not have an overshoot, which might make it more suitable for real-time applications. Additionally, Figure 7a shows that the proposed scenarios $A = 1 \quad \phi = 0^\circ$ relative to other scenarios and PID [25] quickly rejects the injected disturbances into the closed loop with an amplitude of 0.3 at t = 0.02 s. Thus, one might conclude that the proposed method, due to the freedom in the selection of the predefined values of the gain and phase margins, has the flexibility to be tuned by control engineers to generate the desired performances according to the application in hand. This can be seen numerically in Table 1, in which one of the proposed scenarios has at least the smallest values for IAE or TV. The optimal values of the gain and phase margins lie in the ranges $2 \quad 6$ and $30^\circ \quad 60^\circ$, respectively [4]. Therefore, it seems from Table 1 that the proposed method with all the investigated scenarios provides optimum values of the gain and phase margin relative to the PID controller [25], which has a gain margin of less than 2. The numerical observations, given in Table 1, illustrate again how the proposed method is flexible in terms of providing different desired control performances.

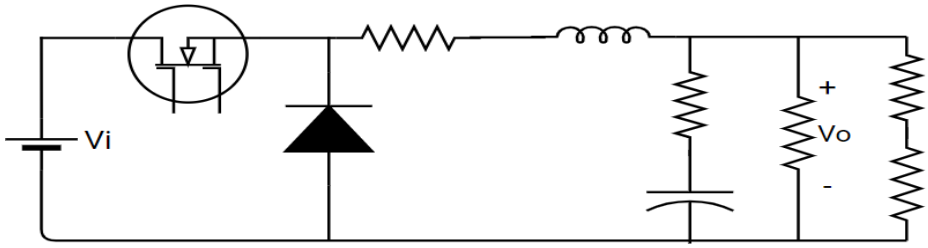

Figure 4. DC–DC buck converter circuit [25].

Table 1. The controller parameters and performance measures for all the studied methods for case study 1.

Method	Controller Parameters				Real Phase and Gain Margins		IAE		TV	
	κ_f	κ_d	κ_p	κ_i	Gain Margin	Phase Margin	Servo	Reg.	Servo	Reg.
Proposed $A = 1 \quad \phi = 0^\circ$	0.539	0.0002	0.104	605.619	2.69	43.48°	0.0011	0.00051	0.00000061	0.0000011
Proposed $A = 1.5 \quad \phi = 0^\circ$	0.539	0.0002	0.069	395.578	2.74	49.23°	0.0016	0.00074	0.00000036	0.0000010
Proposed $A = 1.6 \quad \phi = \pi/4^\circ$	0.539	0.0002	0.170	235.089	2.58	45.18°	0.0028	0.0013	0.00000071	0.0000012
PID [25]	-	0.0004	0.545	626.437	1.75	49.93°	0.0013	0.00066	0.00000041	0.0000022

To evaluate the effectiveness of the approaches under evaluation in the event of a situation where the system parameters change, another test is carried out. This test is particularly important to show how the suggested method gives a robust performance against parameter uncertainties. To show the benefits of incorporating the predefined gain and phase margin boundaries into the proposed method, the system parameters τ, a, b, and c are changed by 500%. The system's parameters are changed by 500% since the reported controllers start to show a noticeable influence. Figure 8 displays the findings of this experiment. It is evident that, in contrast to PID and scenario $A = 1 \quad \phi = 0^\circ$, which display oscillatory behavior and the potential to lose stability, scenarios $A = 1.5 \quad \phi = 0^\circ$

and $A = 1.6$ $\phi = \pi/4°$ maintain system stability with a very small overshoot. To sum up, the suggested scenarios examined in Figures 7 and 8 demonstrate that the suggested approach gives the control engineer the flexibility and opportunity to choose the most suitable control performance, potentially weighing fast-tracking against robust performance in the face of system parameter fluctuations. This possibility is not available in the centroid tuning methods reported in Refs. [3,4,16,18,22], which forms the main contribution of this paper in addition to the analytical nature of the proposed method.

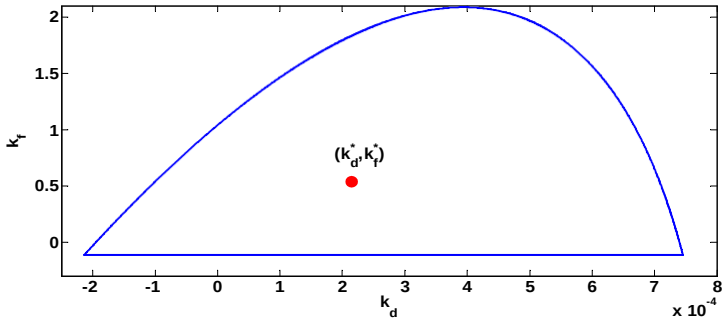

Figure 5. Stability region of the PD controller for Case study 1 for the nominal parameters.

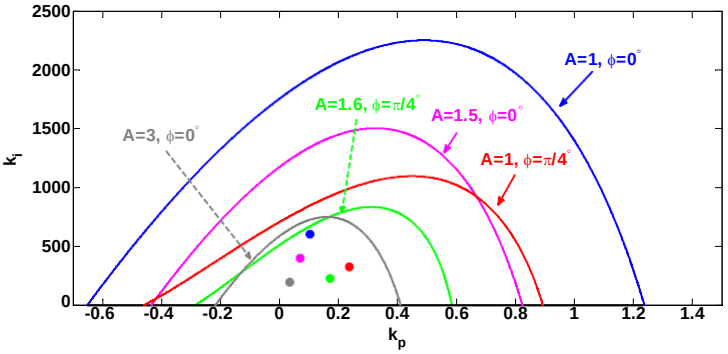

Figure 6. Stability region of the PI controller for Case study 1 for the nominal parameters.

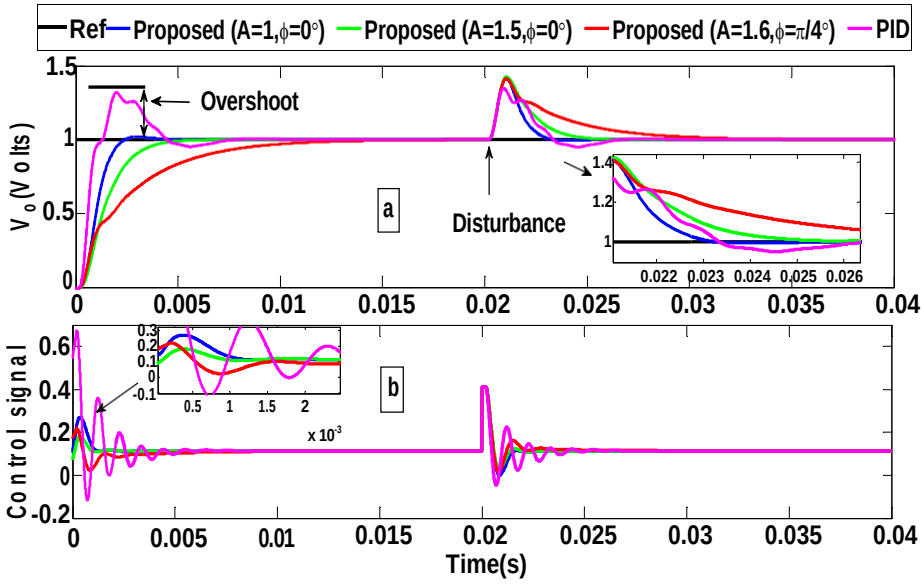

Figure 7. (a) Closed-loop responses for DC–DC buck converter under a 0.3 disturbance amplitudeand for the nominal parameters; (b) corresponding control signals.

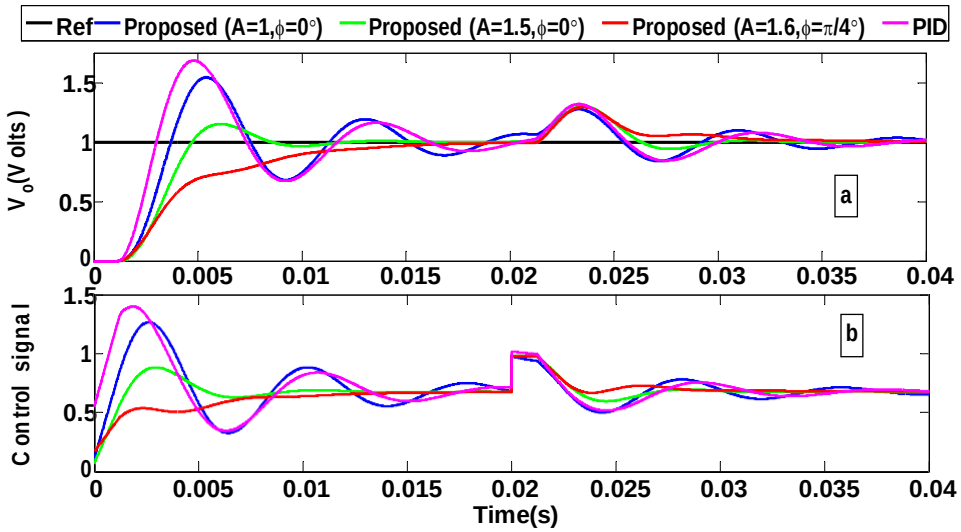

Figure 8. (a) Closed-loop responses for DC–DC buck converter under a 0.3 disturbance amplitudeand 500% model uncertainty; (b) corresponding control signals.

Case study 2: A position control problem for a DC motor is considered in this case study. The identified transfer function of the DC motor position is $G(s) = \frac{0.9843e^{-0.02s}}{0.0651s^2+s}$ [26]. The parameters of the proposed method for the assumed values of $A = 1.3$ $\phi = 0°$ are computed using the steps given in Figure 3. The fractional order PI controller (FOPI) [26] and the PI-PD controller adjusted by CCSR [4] are used to compare the performance with the suggested approach. Table 2 contains a list of all the reported controller settings values together with the values of performance measures.

Table 2. The controller parameters and performance measures for all the studied methods for case study 2.

Method	Controller Parameters					Real Phase and Gain Margins		Step Input				Variable Input	
								IAE		TV		IAE	TV
	k_f	k_d	k_p	k_i	μ	Gain Margin	Phase Margin	Servo	Reg.	Servo	Reg.	Servo	Servo
Proposed (A = 1.3 ϕ = 0°)	38.838	1.866	8.175	300.739	-	2.52	37.3°	0.13	0.003	0.005	0.0005	0.13	0.0048
PI-PD [4]	47.715	2.703	29.818	823.207	-	1.67	22.9°	0.10	0.002	0.058	0.0017	0.09	0.058
FOPI [26]	-	-	12.103	123.761	1.6	0.63	35.9°	0.66	0.115	0.005	0.0007	0.66	0.0048

First of all, the investigated methods are tested using the nominal parameters and by applying a unity response and unity disturbance at t = 0 s and t = 3 s, respectively. Figure 9 displays the outcomes for this test. It is clear from the figure that FOPI [26] has poor performance with oscillatory response and long settling times. On the other hand, the proposed method offers a quick response with zero overshoot and a similar disturbance rejection capability relative to PI-PD [4], which has an oscillatory transient response. Also, the PI-PD [4] consumes more energy relative to the proposed controller as seen in the control signals given in Figure 9b.

The second test for the methods under investigation includes introducing parameter perturbations. By introducing 30% uncertainties in all system parameters, the benefits of incorporating the predetermined gain and phase margin boundaries into the design procedures of the proposed method are demonstrated in Figure 10. From the figure, the suggested strategy is the only one that can continue to function well even when there are fluctuations in the system parameters, while other approaches lose their stability

entirely. This makes the proposed method suitable for controlling systems that have changing parameters.

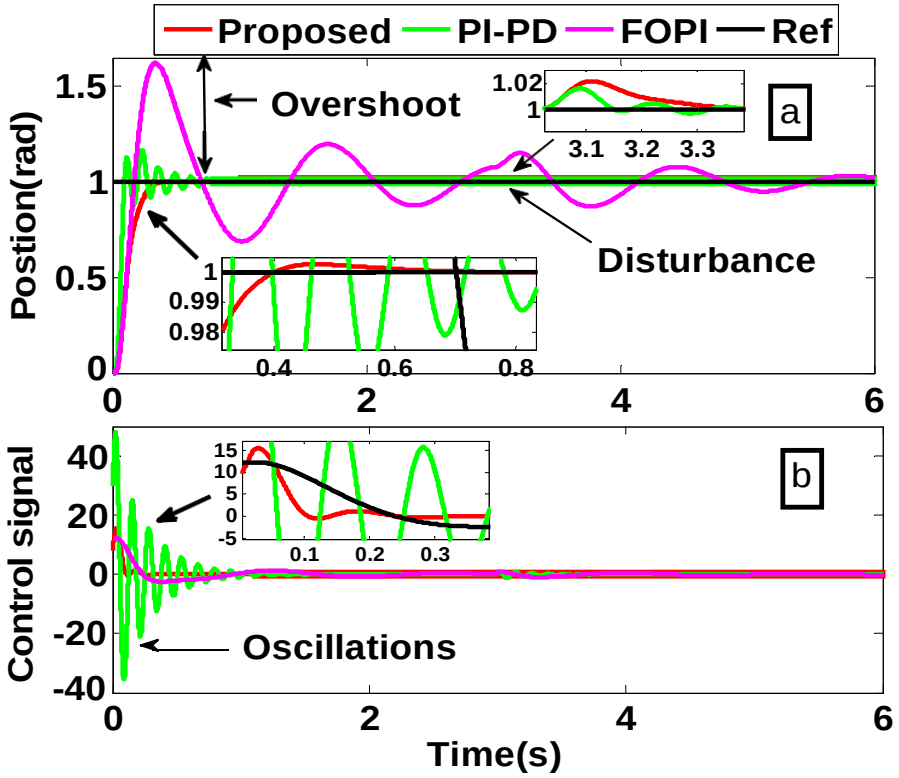

Figure 9. (**a**) Closed-loop responses for DC motor for a step input and under a unity disturbance amplitude for the nominal parameters; (**b**) corresponding control signals.

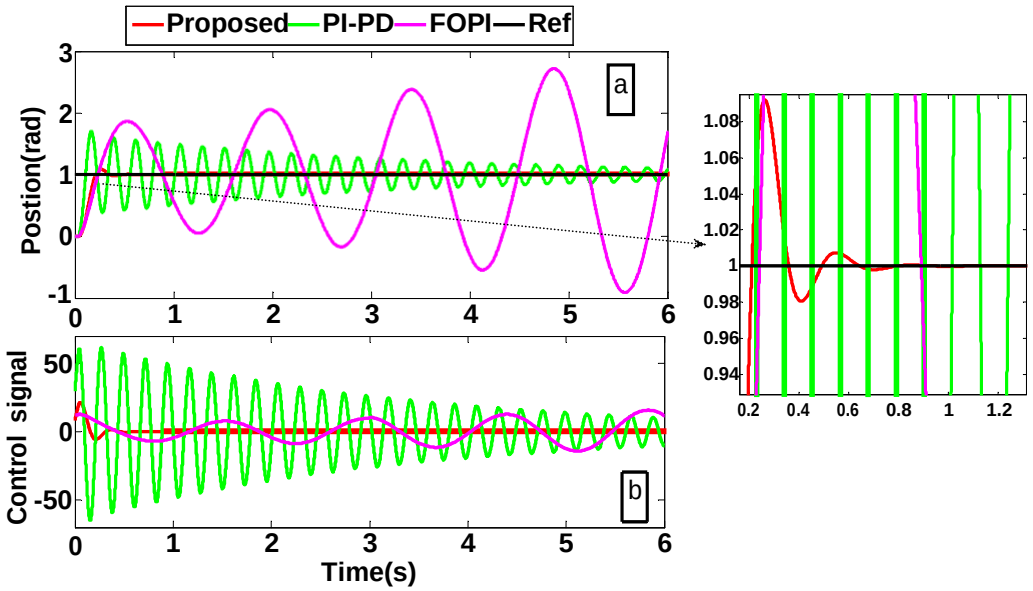

Figure 10. (a) Closed-loop responses for DC motor for a step input and under a unity disturbanceamplitude and 30% model uncertainty; (b) corresponding control signals.

The third test for the reported methods is performed using a variable input consisting of square and sinusoidal signals, as shown in Figure 11a. One can see from the figure that the proposed method has decent performance without introducing oscillations or overshoots. As can be observed from the IAE readings for the variable input given in Table 2, the PI-PD controller [4] provides the fewest tracking errors; but, as Figure 11a,b makes evident, it

exhibits oscillatory transient responses. This might lead to instability in real-time scenarios. Also, the FOPI controller [26] has a response with overshoots and oscillations, as noticeable in Figure 11a. Thus, one can conclude that only the proposed method can give suitable performance without overshoots and oscillations and with reasonable tracking of errors.

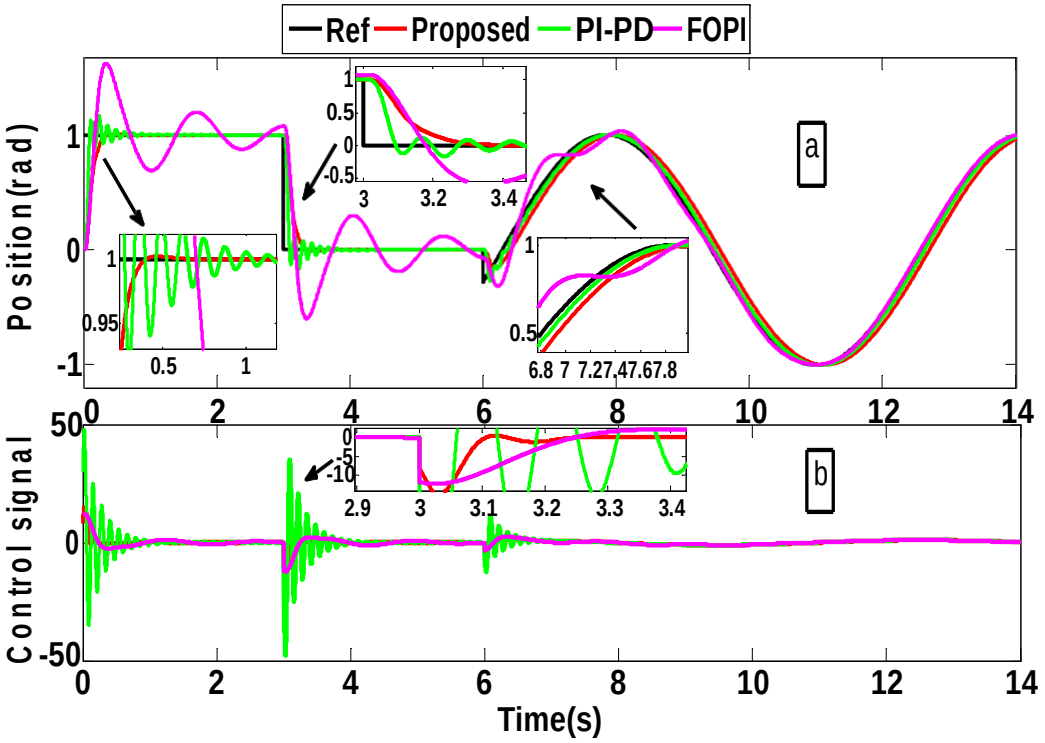

Figure 11. (a) Closed-loop responses for DC motor for a variable input and under the nominal parameters; (b) corresponding control signals.

The TV values, listed in Table 2, show that the proposed method has the smoothest control signal for servo or regulatory responses for both types of control signals. The IAE values presented in the same table demonstrate that, for either servo or regulatory responses, the suggested approach offers a trade-off performance between the strategies described in Refs. [4,26] for all the input types. However, different gain and phase margins might be chosen if control engineers want a different level of intended performance. This is because the suggested method has the flexibility to do so as shown in case study 1. Also, the proposed method has optimal values of the gain and phase margins relative to the other methods as clear from Table 2. To conclude, the above observations demonstrate, yet again, the flexibility, robustness, and importance of the suggested approach.

Case study 3: An industrial temperature control based on a heat exchanger, displayed in Figure 12, is considered under this case study. A shell-and-tube system is used to transfer the heat from a primary to a secondary flow. The process control goal is to maintain the secondary flow point's temperature by regulating the primary flow. The system's recognized transfer function is $G(s) = \frac{0.002e^{-3s}}{s}$ [2]. By following the methods shown in Figure 3, one can calculate the settings of the suggested technique for assumed scenarios of $A = 1$ $\phi = 0^\circ$ and $A = 1.3$ $\phi = 0^\circ$. The values of these settings are summarized in Table 3, together with the reported values of the PI-PD controller plus the Smith predictor reported in reference [2]. PI-PD-SP is the abbreviation for the PI-PD controller plus the Smith predictor [2] in this case study. The goal of the comparison between the proposed method and PI-PD-SP is to show that the proposed method can perform well in the presence of long time delays, even though it has not incorporated another technique for handling the long time delay such as the Smith predictor.

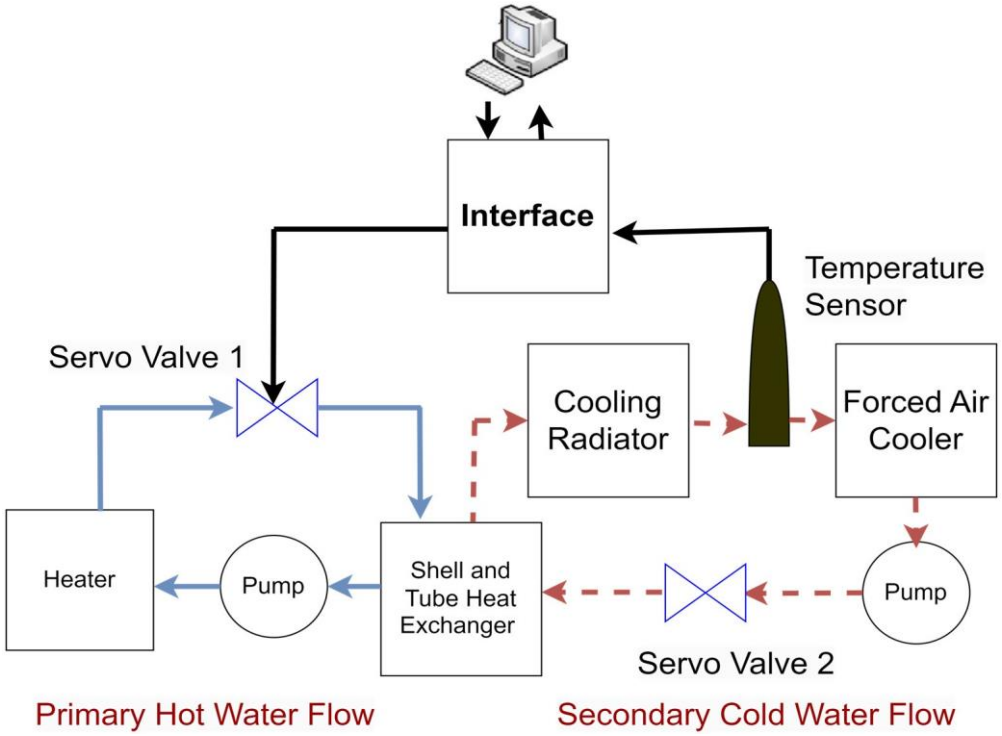

Figure 12. Diagrammatic representation of temperature control using a heat exchanger.

Table 3. The controller parameters and performance measures for Case study 3.

Method	Controller Parameters				Real Phase and Gain Margins		Step Input				Square Input	
							IAE		TV		IAE	TV
	k_f	k_d	k_p	k_i	Gain Margin	Phase Margin	Servo	Reg.	Servo	Reg.	Servo	Servo
Proposed (A = 1 ϕ = 0°)	83.34	0	22.762	8.113	2.18	32.63°	10.272	0.370	0.014	0.0013	30.817	0.028
Proposed (A = 1.5 ϕ = 0°)	83.34	0	15.175	5.409	2.45	39.87°	15.408	0.555	0.009	0.0011	46.203	0.042
PI-PD-SP [2]	130.15	188.326	26.011	25.601	1.93	27.85°	5.184	0.120	0.029	0.0018	15.553	0.086

Different tests are performed to test the proposed method. In the first test, a unity step input and disturbance with an amplitude of 3 are applied at t = 0 s and t = 80 s, respectively. The outcomes of this test are shown in Figure 13. The second test includes introducing variable input in the form of square input as shown in Figure 14. The third test is similar to the first one but after introducing 70% model uncertainty in the time delay. Its results are shown in Figure 15. The following observations are noted based on Figures 13–15, as well as the performance metrics listed in Table 3:

1. As seen in Figures 13 and 14, the suggested scenario, $A = 1$ $\phi = 0°$, provides somewhat similar responses and results to the PI-PD-SP controller [2], even though it does have an additional mechanism to tackle long time delays.
2. In contrast to PI-PD-SP [2], which completely loses stability under 70% variations in the time delay as clear in Figure 15, the suggested scenarios $A = 1$ $\phi = 0°$ and $A = 1.3$ $\phi = 0°$ can keep the system stable with a satisfactory performance. Also,

the robustness of the proposed method can be numerically seen from the real values of the gain and phase margin provided in Table 3.

3. As can be observed from the TV values listed in Table 3, the suggested scenarios provide smoother control signals. Furthermore, as shown in Figures 13b and 14b, the suggested method uses less control power for the transient response than the PI-PD-SP [2].

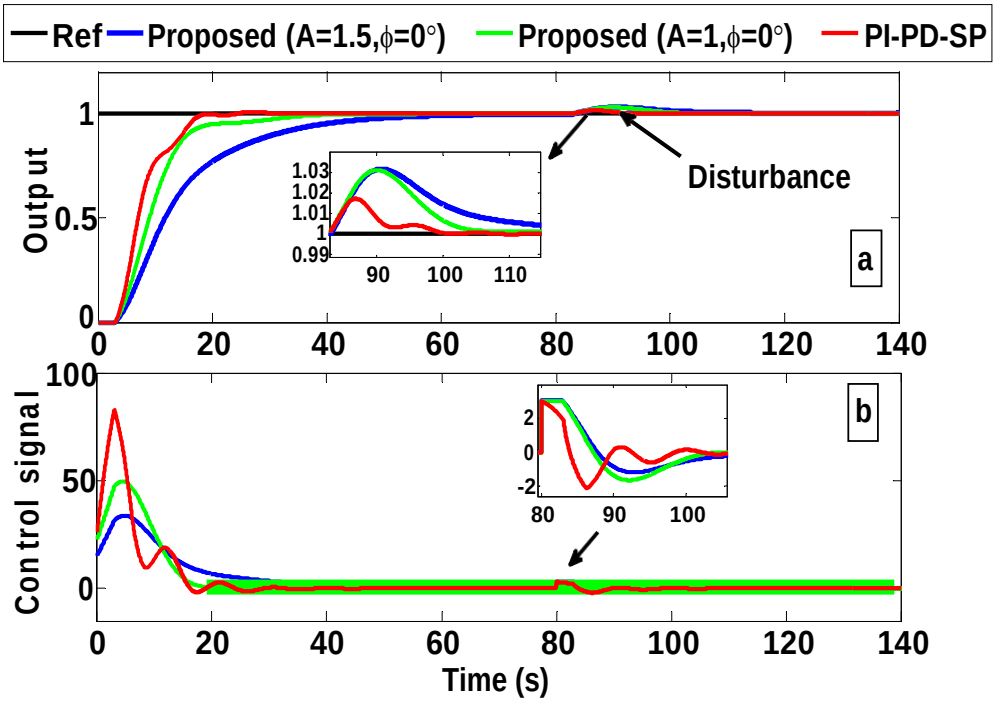

Figure 13. (a) Closed-loop responses for the temperature control for a step input and under thenominal parameters; (b) corresponding control signals.

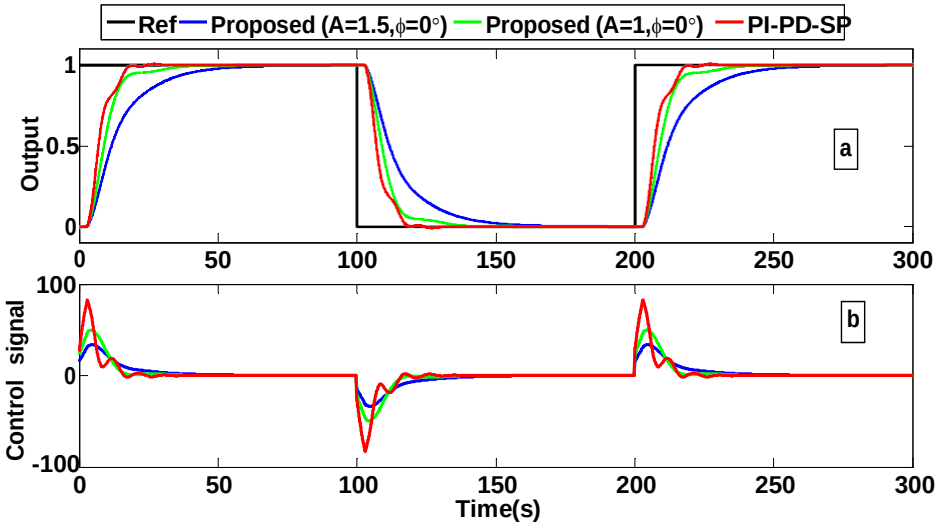

Figure 14. (a) Closed-loop responses for the temperature control for a square input and under thenominal parameters; (b) corresponding control signals.

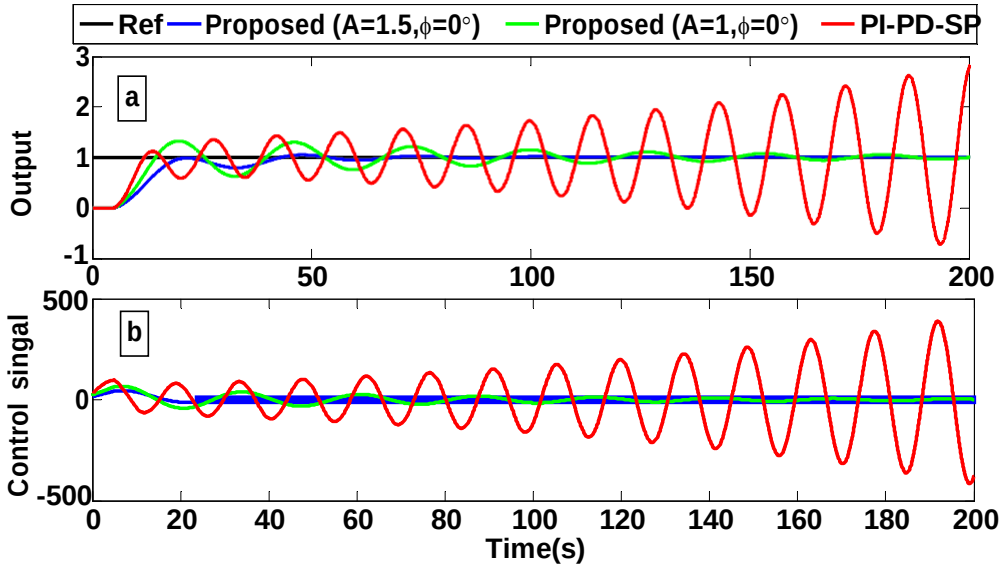

Figure 15. (a) Closed-loop responses for the temperature control under a unity disturbance amplitudeand 70% time delay model uncertainty; (b) corresponding control signals.

Experimental results: Here, the proposed technique is tested using a real-time trial on a TRMS. The dynamics of the nonlinear TRMS system are comparable to those of a helicopter. As seen in Figure 16, it comprises two DC motors that drive the pitch and yaw propellers at the ends of a beam. The yaw rotor produces horizontal revolution on the yaw axis, whilst the pitch rotor is in charge of the upward motion on the pitch axis. There is a noticeable cross-coupling between the rotor's actions, with each rotor affecting both angles. The yaw transfer function of yaw angle is identified as $G(s) = \frac{0.10e^{-0.3227s}}{0.95965s^2+s}$ [4]. On the other hand, the transfer function of the pitch angle is identified using the input and output data as $G(s) = \frac{0.32e^{-s}}{2.347s^2+0.1s+1}$.

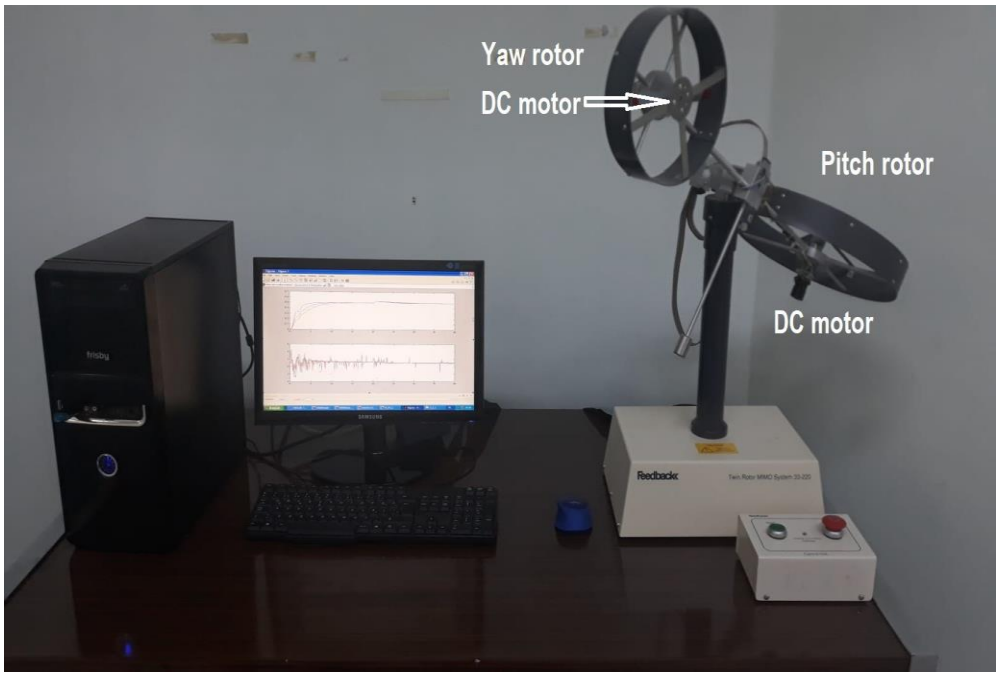

Figure 16. TRMS setup.

The suggested method in Figure 3 is used to compute the settings of the yaw and pitch PI-PD controllers using the assumed scenarios $A = 1 \quad \phi = 0°$ and $A = 1 \quad \phi = \pi/3.7°$,

respectively. The proposed controller is implemented using the diagram shown in Figure 17. The PID controller described in Ref. [27] is contrasted with the suggested approach. Table 4 displays the IAE values together with the parameters for every method that has been reported. To ensure a fair comparison, it is vital to note that every controller evaluated is subjected to identical implementation conditions. An example of these conditions might include the absence of external disturbances such as wind.

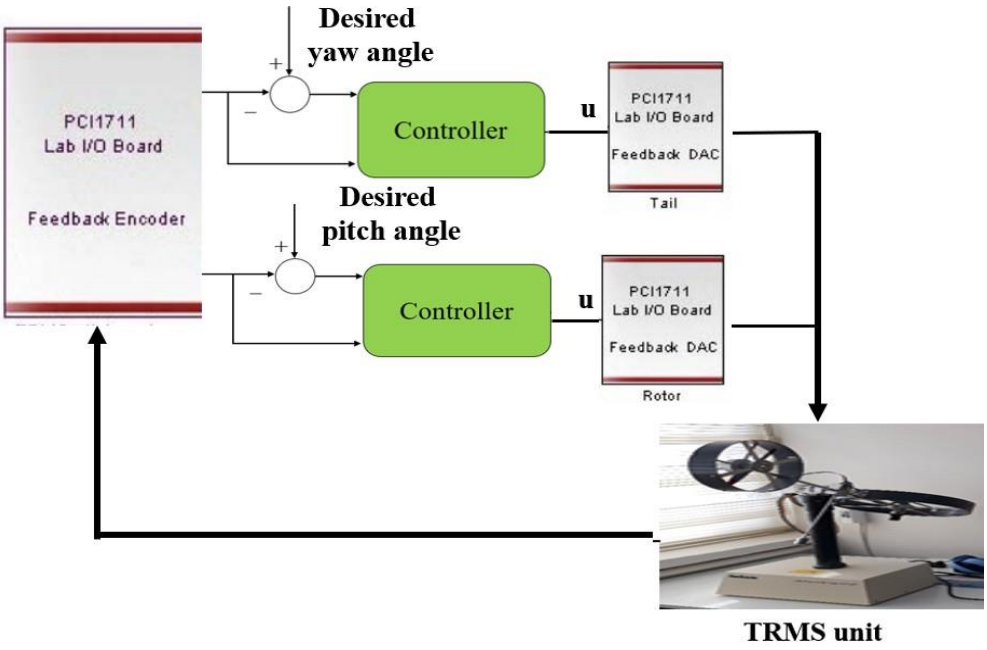

Figure 17. Diagram for implementing the PI-PD controller.

Table 4. The controller parameters and IAEs for all the studied methods for the real-time test.

Method		Controller Parameters				IAE
		k_f	k_d	k_p	k_i	
Proposed	Yaw controller $A = 1 \quad \phi = 0^\circ$	22.4563	16.6002	6.1352	14.0555	0.9711
	Pitch controller $A = 1 \quad \phi = \pi/3.7^\circ$	0.1122	2.6569	0.1959	1.1341	1.7484
PID [27]	Yaw controller	-	5	2	1	1.7774
	Pitch controller	-	10	5	6	1.2817

The real-time outcomes for concurrently controlling the pitch and yaw angles are shown in Figures 18 and 19. The simulation outcomes for the suggested method are also displayed in Figures 18a and 19a. Interestingly, the proposed method yields somewhat similar real-time and simulation results, even though the TRMS is a highly nonlinear system with coupling effects that may be challenging to model using low-order transfer functions. The suggested approach exhibits rapid responses with shorter settling times and overshoot, particularly for the yaw response, as seen in Figure 18. Additionally, Figures 18b and 19b demonstrate how much less energy the suggested controller uses than the PID controller [27]. Furthermore, even though the suggested approach is primarily suggested for single-input single-output systems, the suggested controller could continue to function well considering the existence of coupling influences between yaw and pitch angles. This is explained by the flexibility of the suggested approach, which enables the designer to use predetermined gain and phase margin boundaries to achieve the desired performance.

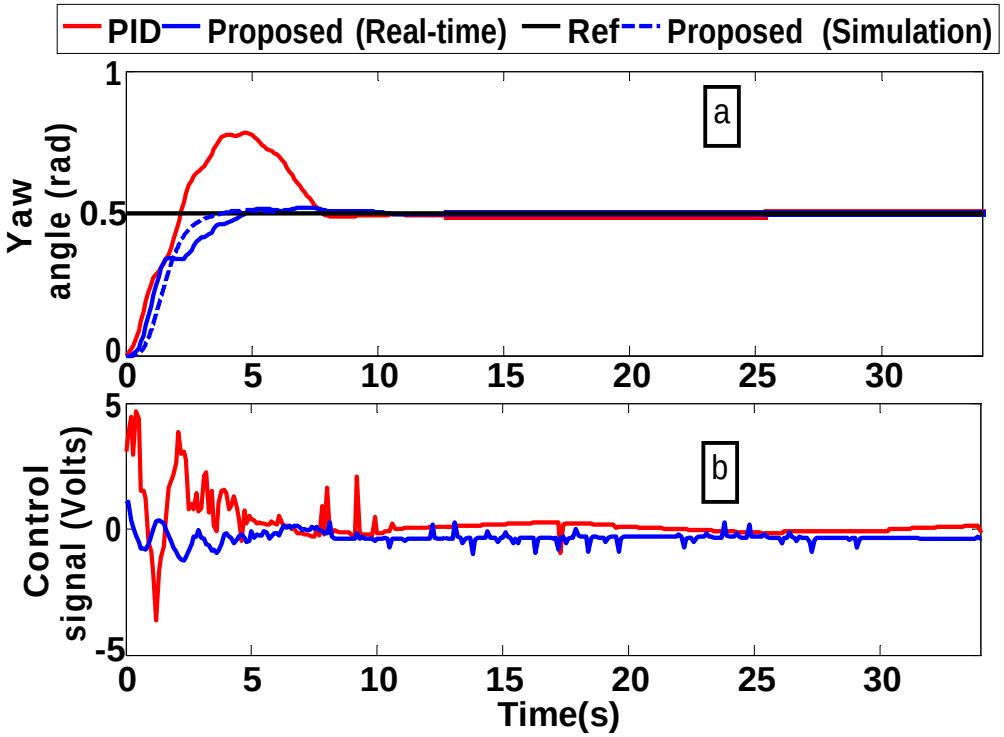

Figure 18. (**a**) Real-time closed-loop yaw responses for TRMS and (**b**) corresponding control signals.

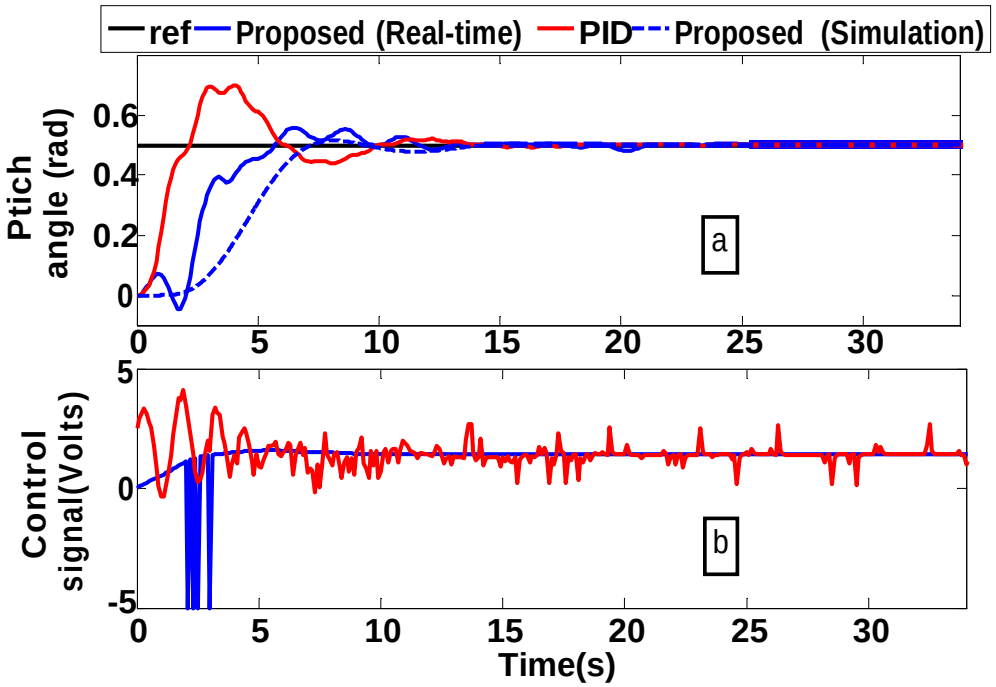

Figure 19. (a) Real-time closed-loop pitch responses for TRMS and (b) corresponding control signals.

5. Conclusions

A robust centroid point design technique based on predefined phase and gain margins is presented in this paper. In comparison to the existing literature, the suggested approach is both analytical and robust. The control engineer has the flexibility to choose the required control performance according to the suggested approach. The analytical centroid point techniques described in the literature really lack this feature. The results of the simulations demonstrated that the suggested approach produces responses with reduced overshoots

and settling times and performs well against parameter uncertainties. These findings are further supported by the results of the real-time test on TRMS, which shows that the proposed methodology can handle the coupling effects to larger levels when utilized for controlling multiple input and multiple output systems even if it is originally only designed to deal with single-input and single-output systems. Nonetheless, the coupling effects continue to influence the pitch angle control performance, albeit to a lesser extent. Future studies will therefore involve extending the suggested approach to handle the coupling effects in multiple-input and multiple-output systems.

List of Symbols

Symbol	Explanation
K	Process gain
τ	Time delay
a, b, c	Coefficients of the process transfer function
$G(s)$	Process transfer function
$G_{PD}(s)$	PD controller's transfer function
$G_{PI}(s)$	PI controller's transfer function
k_f	The proportional gain of the PD controller
k_d	The derivative gain of the PD controller
k_p	The proportional gain of the PI controller
k_i	The integral gain of the PI controller
A	Gain margin
θ	Phase margin
ω_{PD}	The critical frequency of the inner loop
ω_{PI}	The critical frequency of the outer loop
$e \quad f$	The minimum and maximum integral limits
$\overline{x}$	The centroid coordinate on the x-axis
$\overline{y}$	The centroid coordinate on the y-axis
μ	The degree of integral operator

REFERENCES

1. Alyoussef, F.; Kaya, I. Improved adaptive dynamic non-singular terminal sliding mode controller with fractional disturbance observer. *Inf. Sci.* **2023**, *641*, 119110. [CrossRef]
2. Singha, P.; Das, D.; Chakraborty, S.; Lloyds Raja, G. Experimentally validated predictive PI-PD control strategy for delay-dominant chemical processes. *Chem. Eng. Sci.* **2024**, *295*, 120197. [CrossRef]
3. Alyoussef, F.; Kaya, I. Novel Tuning Rules for Adjusting the Parameters of the PI-PD Controller for Controlling Unstable Processes. *Adv. Transdiscipl. Eng.* **2024**, *46*, 254–261.
4. Alyoussef, F.; Kaya, I. Simple PI-PD tuning rules based on the centroid of the stability region for controlling unstable and integrating processes. *ISA Trans.* **2023**, *134*, 238–255. [CrossRef] [PubMed]
5. Kaya, I. I-PD Controller Design for Integrating Time Delay Processes Based on Optimum Analytical Formulas. *IFAC-PapersOnLine* **2018**, *51*, 575–580. [CrossRef]
6. Zou, H.; Li, H. Improved PI-PD control design using predictive functional optimization for temperature model of a fluidized catalytic cracking unit. *ISA Trans.* **2017**, *67*, 215–221. [CrossRef]
7. Lloyds Raja, G.; Ali, A. New PI-PD Controller Design Strategy for Industrial Unstable and Integrating Processes with Dead Time and Inverse Response. *J. Control Autom. Electr. Syst.* **2021**, *32*, 266–280. [CrossRef]
8. Mahapatro, S.R.; Subudhi, B. A New H∞ Weighted Sensitive Function-Based Robust Multi-Loop PID Controller for a Multi-Variable System. *IEEE Trans. Circuits Syst. II Express Briefs* **2024**, *71*, 1256–1260. [CrossRef]
9. Jain, C.; Vaishnav, N.; Jain, A.K. MTPA Control of Double Inverter Fed Wound Rotor Induction Motor Drive. *IEEE Trans. Energy Convers.* **2023**, *38*, 2326–2343. [CrossRef]
10. Vaishnav, N.; Jain, A. Stabilizing Sets of Current PI Controllers for IM Drives with and without LC Filter. *IEEE Trans. Energy Convers.* **2022**, *37*, 958–969. [CrossRef]
11. Mehta, U.; Aryan, P.; Raja, G.L. Tri-Parametric Fractional-Order Controller Design for Integrating Systems with Time Delay. *IEEE Trans. Circuits Syst. II Express Briefs* **2023**, *70*, 4166–4170. [CrossRef]
12. Onat, C. A new design method for PI–PD control of unstable processes with dead time. *ISA Trans.* **2019**, *84*, 69–81. [CrossRef] [PubMed]
13. Ozyetkin, M.M.; Onat, C.; Tan, N. PI-PD controller design for time delay systems via the weighted geometrical center method. *Asian J. Control* **2020**, *22*, 1811–1826. [CrossRef]
14. İrgan, H.; Menak, R.; Tan, N. A comparative study on PI-PD controller design using stability region centroid methods for unstable, integrating and resonant systems with time delay. *Meas. Control* **2024**. [CrossRef]

15. Imran Kalim, M.; Ali, A. New tuning strategy for series cascade control structure. *IFAC-PapersOnLine* **2020**, *53*, 195–200. [CrossRef]
16. Alyoussef, F.; Kaya, I. Tuning proportional-integral controllers based on new analytical methods for finding centroid of stability locus for stable/unstable first-order plus dead-time processes. *Proc. Inst. Mech. Eng. Part I J. Syst. Control Eng.* **2022**, *236*, 818–831. [CrossRef]
17. Ozyetkin, M.M. An approximation method and PID controller tuning for systems having integer order and non-integer order delay. *Alex. Eng. J.* **2022**, *61*, 11365–11375. [CrossRef]
18. Alyoussef, F.; Kaya, I. Proportional–integral and proportional–derivative controller design based on analytically computed centroid point for controlling integrating processes. *Proc. Inst. Mech. Eng. Part I J. Syst. Control Eng.* **2023**, *237*, 1045–1065. [CrossRef]
19. Yildirim, B.; Gheisarnejad, M.; Khooban, M.H. A Robust Non-Integer Controller Design for Load Frequency Control in Modern Marine Power Grids. *IEEE Trans. Emerg. Top. Comput. Intell.* **2021**, *6*, 852–866. [CrossRef]
20. Yildirim, B.; Gheisarnejad, M.; Khooban, M.H. A New Parameter Tuning Technique for Noninteger Controllers in Low-Inertia Modern Power Grids. *IEEE J. Emerg. Sel. Top. Ind. Electron.* **2021**, *3*, 279–288. [CrossRef]
21. Kalim, M.I.; Ali, A. A graphical approach for controller design with desired stability margins for a DC–DC boost converter. *IET Power Electron.* **2021**, *14*, 1323–1335. [CrossRef]
22. Çökmez, E.; Kaya, İ. An analytical solution of fractional order PI controller design for stable/unstable/integrating processes with time delay. *Turk. J. Electr. Eng. Comput. Sci.* **2023**, *31*, 626–645. [CrossRef]
23. Tan, N. Computation of stabilizing PI-PD controllers. *Int. J. Control Autom. Syst.* **2009**, *7*, 175–184. [CrossRef]
24. Kumar, S.R.; Anwar, M.N.; Verma, P.; Ram, M.K.; Somanshu, S.R. H∞ Criterion Based PI Controller Design for DC-DC Step-Up Converters. *IEEE J. Emerg. Sel. Top. Ind. Electron.* **2023**, *5*, 402–413. [CrossRef]
25. Ramana, K.V.; Majhi, S.; Gogoi, A.K. Modeling and Estimation of DC-DC Buck Converter Dynamics Using Relay Feedback Output with Performance Evaluation. *IEEE Trans. Circuits Syst. II Express Briefs* **2019**, *66*, 427–431.
26. Lino, P.; Maione, G.; Stasi, S.; Padula, F.; Visioli, A. Synthesis of fractional-order PI controllers and fractional-order filters for industrial electrical drives. *IEEE/CAA J. Autom. Sin.* **2017**, *4*, 58–69. [CrossRef]
27. Alyoussef, F.; Kaya, I. TRMS Experimental Results of New Nonlinear PID Tuned by de Algorithm. In Proceedings of the 2019 3rd International Conference on Applied Automation and Industrial Diagnostics, ICAAID 2019, Elazig, Turkey, 25–27 September 2019.